

A SCALE-DEPENDENT DYNAMIC MODEL FOR SCALAR TRANSPORT IN LARGE-EDDY SIMULATIONS OF THE ATMOSPHERIC BOUNDARY LAYER

FERNANDO PORTÉ-AGEL^{1,2}

¹*St. Anthony Falls Laboratory, Department of Civil Engineering, University of Minnesota, Minneapolis, MN 55414, U.S.A.;* ²*National Center for Earth-Surface Dynamics*

(Received in final form 31 July 2003)

Abstract. An important challenge in large-eddy simulations of the atmospheric boundary layer is the specification of the subgrid-scale (SGS) model coefficient(s) and, in particular, how to account for factors such as position in the flow, grid/filter scale and atmospheric stability. A dynamic SGS model (that assumes scale invariance of the coefficients) is implemented in simulations of a neutral boundary layer with a constant and uniform surface flux of a passive scalar. Results from our simulations show evidence that the lumped coefficient in the eddy-diffusion model computed with the dynamic procedure depends on scale. This scale dependence is stronger near the surface, and it is more important for the scalar than for the velocity field (Smagorinsky coefficient) due to the stronger anisotropic behaviour of scalars. Based on these results, a new scale-dependent dynamic model is developed for the eddy-diffusion lumped coefficient. The new model, which is similar to the one proposed earlier for the Smagorinsky coefficient, is fully dynamic, thus not requiring any parameter specification or tuning. Simulations with the scale-dependent dynamic model yield the expected trends of the coefficients as functions of position and filter/grid scale. Furthermore, in the surface layer the new model gives improved predictions of mean profiles and turbulence spectra as compared with the traditional scale-invariant dynamic model.

Keywords: Atmospheric boundary layer, Large-eddy simulation, Passive scalar, Subgrid-scale modeling, Turbulence.

1. Introduction

Large-eddy simulation (LES) is becoming an increasingly popular tool to study turbulent transport in the atmospheric boundary layer (ABL, e.g., Moeng, 1984; Nieuwstadt et al., 1991; Shaw and Schumann, 1992; Andren et al., 1994; Sullivan et al., 1994; Kosovic, 1997; Avissar and Schmidt, 1998; Albertson and Parlange, 1999; Porté-Agel et al., 2000; Lin and Glendening, 2002). LES explicitly resolves the dynamics of the flow for all turbulent scales larger than the grid size Δ_{grid} (on the order of 10 m in the ABL), while the contribution of the subgrid-scale physics is parameterized. Subgrid-scale (SGS) modelling constitutes a major challenge in LES due to the fact that simulation results are very sensitive to (a) the subgrid-scale model formulation, and (b) the way the model coefficients are specified (Meneveau and Katz, 2000; Piomelli, 1999; Piomelli and Balaras, 2002).



Boundary-Layer Meteorology **112**: 81–105, 2004.

© 2004 Kluwer Academic Publishers. Printed in the Netherlands.

In LES the separation of scales between resolved and subgrid scales is achieved by filtering (with a filter of characteristic width $\Delta \geq \Delta_{grid}$) the equations describing the transport of momentum and scalar quantities. For a scalar θ , the effect of the unresolved scales (smaller than Δ) on the evolution of the filtered scalar concentration $\tilde{\theta}$ appears through the SGS flux q_i , which is defined as

$$q_i = \widetilde{u_i \theta} - \widetilde{u}_i \widetilde{\theta}. \quad (1)$$

Note that q_i needs to be parameterized (using a SGS model) as a function of the resolved (filtered) velocity and scalar fields. In the near-ground region of wall-bounded turbulent flows, such as the ABL, the characteristic eddy size is relatively small compared to the grid/filter scale, making the subgrid-scale fluxes a large fraction of the overall turbulent fluxes. Moreover, near the ground the flow becomes more anisotropic at all resolved scales (including the grid scale) as the filter scale falls near (or even outside) the upper limit of the inertial subrange. This is expected to affect the performance of most SGS models that assume, in one way or another, isotropic behaviour at the subgrid scales and at the smallest resolved scales. In particular, dynamic models, used to optimize the value of the model coefficient(s) based on the information contained in the resolved scales, rely on the assumption of isotropy of the flow and scale invariance of the model coefficients at the smallest resolved scales (Germano et al., 1991; Moin et al., 1991; Lilly, 1992). In a recent a priori field study, Porté-Agel et al. (2001) showed experimental evidence of scale dependence of the coefficient in the eddy-viscosity and eddy-diffusion models. This is consistent with results from a numerical study (Porté-Agel et al., 2000) that shows scale dependence of the eddy-viscosity coefficient computed using the dynamic model. In general, scale dependence was found to be more important near the ground, and stronger with increasing Δ/z ratio (where z is the distance to the ground).

In this paper, we address the issue of scale dependence in the eddy-diffusion model (for the SGS scalar flux). In Section 2 we show evidence, from numerical simulations with the standard dynamic model, that near the ground the model coefficient strongly depends on the grid/filter scale. In Section 3 we introduce a new dynamic procedure (thus not requiring any parameter specification) that accounts for the scale dependence of the coefficient based on information contained in the resolved field. The new scale-dependent model is tested in simulations of a neutral atmospheric boundary layer with a constant surface flux of a passive scalar.

2. The Dynamic Model

2.1. MODEL FORMULATION

The eddy-diffusion model is widely used in LES of the atmospheric boundary layer. A common formulation of this model is

$$q_i^{ed} = - [Sc_{sgs}^{-1} C_S^2 (\Delta)] \Delta^2 |\tilde{S}| \frac{\partial \tilde{\theta}}{\partial x_i}, \quad (2)$$

where $|\tilde{S}| = (2\tilde{S}_{ij}\tilde{S}_{ij})^{1/2}$ is the resolved strain-rate magnitude and \tilde{S}_{ij} is the resolved strain rate tensor; $Sc_{sgs}^{-1} C_S^2$ is a lumped coefficient that comprises the Smagorinsky coefficient C_S in the eddy-viscosity model, and the subgrid-scale Schmidt number Sc_{sgs} . Note that if θ is temperature, then $Sc_{sgs} = Pr_{sgs}$, the subgrid-scale Prandtl number.

The value of the model parameters C_S and Sc_{sgs} (and therefore $Sc_{sgs}^{-1} C_S^2$) is well established for isotropic turbulence. In that case, if a cut-off filter is used in the inertial subrange and the filter scale Δ is equal to the grid size Δ_{grid} , then $C_S \approx 0.17$ and $Sc_{sgs} \approx 0.4$ (Lilly, 1967; Mason and Derbyshire, 1990). However, anisotropy of the flow and the presence of a strong mean shear near the surface in high Reynolds number boundary layers makes the optimum value of those coefficients depart from their isotropic counterparts.

Several efforts have been made to account for the effect of flow anisotropy (due to mean shear and stable stratification) on SGS model coefficients (Deardorff, 1971, 1980; Hunt et al., 1988; Schumann, 1991; Canuto and Cheng, 1997; Kleissl et al., 2003). Most of the proposed formulations account for shear and stability corrections in the Smagorinsky coefficient with an ad hoc function of non-dimensional shear and stability parameters. The trend in those models is that the coefficient decreases to account for the increased flow anisotropy and reduced characteristic eddy size associated with large values of shear and/or stability (see e.g., Figure 3 of Canuto and Cheng, 1997).

Another more systematic way to obtain the SGS model coefficient(s) is using so-called dynamic procedures. Dynamic models avoid the need for a priori specification and consequent tuning of coefficients because they are evaluated directly from the resolved scales in LES (Germano et al., 1991; Moin et al., 1991; Lilly, 1992; Meneveau and Katz, 2000). For scalar fluxes, the dynamic procedure is based on the identity

$$K_i = Q_i - \bar{q}_i = \overline{\tilde{u}_i \tilde{\theta}} - \tilde{u}_i \tilde{\theta}, \quad (3)$$

where $Q_i = \overline{\tilde{u}_i \tilde{\theta}} - \tilde{u}_i \tilde{\theta}$ is the SGS flux at a test-filter scale (typically $\bar{\Delta} = 2\Delta$) and K_i is a 'resolved flux' vector that can be evaluated based on the resolved scales. Applying the eddy-diffusion model, Q_i is determined by

$$Q_i = - [Sc_{sgs}^{-1} C_S^2 (\bar{\Delta})] \bar{\Delta}^2 |\bar{S}| \frac{\partial \bar{\theta}}{\partial x_i}. \quad (4)$$

Substitution of Equations (2) and (4) into (3) leads to the system

$$K_i = Sc_{sgs}^{-1} C_S^2 X_i, \quad (5)$$

where, for $\overline{\Delta} = 2\Delta$,

$$X_i = \Delta^2 \left(\overline{|\tilde{S}|} \frac{\partial \overline{\theta}}{\partial x_i} - 4 \frac{Sc_{sgs}^{-1} C_S^2 (2\Delta)}{Sc_{sgs}^{-1} C_S^2 (\Delta)} \overline{|\tilde{S}|} \frac{\partial \overline{\theta}}{\partial x_i} \right). \quad (6)$$

It is important to note that the traditional dynamic model assumes scale invariance of the model coefficient at the filter and test filter scales, i.e.,

$$Sc_{sgs}^{-1} C_S^2 (\Delta) = Sc_{sgs}^{-1} C_S^2 (\overline{\Delta}) = Sc_{sgs}^{-1} C_S^2. \quad (7)$$

Minimizing the error associated with the use of the eddy-diffusion model in Equation (3) over all three vector components, as well as over some averaging region of statistical homogeneity (Ghosal et al., 1995) or fluid pathlines (Meneveau et al., 1996), results in

$$Sc_{sgs}^{-1} C_S^2 = \frac{\langle K_i X_i \rangle}{\langle X_i X_i \rangle}. \quad (8)$$

Although widely used in the engineering community to compute the Smagorinsky coefficient (for a review, see Meneveau and Katz, 2000), the dynamic model has not yet become common practice in simulations of the atmospheric boundary layer. In a recent study, Porté-Agel et al. (2000) applied a dynamic model to compute C_S in simulations of a neutral boundary layer. They showed that, as opposed to the traditional eddy-viscosity model that is too dissipative near the ground, the dynamic model is not dissipative enough, leading to velocity gradients that are too small near the ground. They also showed that near the ground the value of C_S obtained from simulations depends on resolution, which constitutes an internal inconsistency of the dynamic model that assumes scale invariance of the coefficient. This result led them to introduce a modification to the dynamic model to allow for scale dependence. The new scale-dependent dynamic model yielded improved turbulence statistics (e.g., mean velocities and velocity spectra) compared with its scale-invariant counterpart. Next, we apply the dynamic model (Equation (8)) to compute $Sc_{sgs}^{-1} C_S^2$ in simulations of a neutral boundary layer with a constant surface flux of a passive scalar with the purpose of evaluating the performance of the dynamic model and also studying the issue of scale dependence of the coefficient.

2.2. NUMERICAL SIMULATIONS

We implement the dynamic eddy-viscosity and dynamic eddy-diffusion models in the simulation of a neutrally stable (no convective forcing) atmospheric boundary

layer with a constant and uniform surface flux of a passive scalar. We use a modified version of the LES code described by Albertson and Parlange (1999) and Porté-Agel et al. (2000). A brief summary of the code is given below.

The code solves the filtered Navier–Stokes equations written in rotational form (Orzag and Pao, 1974) as well as the conservation equation for the filtered scalar concentration:

$$\frac{\partial \tilde{u}_i}{\partial t} + \tilde{u}_j \left(\frac{\partial \tilde{u}_i}{\partial x_j} - \frac{\partial \tilde{u}_j}{\partial x_i} \right) = -\frac{\partial \tilde{p}^*}{\partial x_i} - \frac{\partial \tau_{ij}}{\partial x_j} + F_i, \quad (9)$$

$$\frac{\partial \tilde{\theta}}{\partial t} + \tilde{u}_j \frac{\partial \tilde{\theta}}{\partial x_j} = -\frac{\partial q_j}{\partial x_j}, \quad (10)$$

where t is time, \tilde{u}_i is the instantaneous resolved velocity in the i -direction, $\tilde{p}^* = \tilde{p} + \frac{1}{2}\tilde{u}_i^2$ is the dynamic pressure, τ_{ij} is the SGS stress tensor, and F_i is a forcing term. In particular, F_i is a constant pressure gradient in the streamwise direction that drives the flow. Since the Reynolds number of the ABL is high and no near-ground viscous processes are resolved, the viscous term is neglected in the momentum equation. Since this paper focuses on the case of neutral stability conditions, no additional terms are used to account for buoyancy effects. Also no Coriolis force has been included.

The code is pseudospectral, i.e., derivatives in the horizontal directions are computed using spectral (Fourier) methods, while vertical derivatives are approximated with second-order central differences. The grid planes are staggered in the vertical, with the first vertical velocity plane at a distance $\Delta_z = L_z/(N_z - 1)$ from the surface, and the first horizontal velocity and temperature plane at $\Delta_z/2$ from the surface.

The computational domain is of size (L_x, L_y, L_z) and it is divided into N_x , N_y , and N_z uniformly spaced grid points. The height of the domain is $L_z = 1000$ m, which corresponds to the height of the boundary layer (H), and the horizontal dimensions of the simulated volume are $L_x = L_y = 2\pi L_z$. The filter width Δ in Equation (2) is computed using the common formulation $\Delta = (\Delta_x \Delta_y \Delta_z)^{\frac{1}{3}}$. Test filtering at scale 2Δ used in the dynamic model is performed using a two-dimensional spectral cut-off filter applied in the horizontal directions. The dynamic procedure used to compute the coefficients is applied for every horizontal plane (averaging over horizontal directions) only once every 10 time steps, taking about 4% of the total CPU time.

De-aliasing of the non-linear products in the convective terms and also in the SGS model terms is performed in Fourier space using the 3/2 rule (Canuto et al., 1988). Time advancement is done using a second-order explicit Adams-Bashforth scheme, which is common in LES (Canuto et al., 1988).

Finite differencing in the vertical requires boundary conditions at the surface and upper boundaries. The upper boundary has a stress/flux free condition, i.e.,

$\partial\tilde{u}_1/\partial z = \partial\tilde{u}_2/\partial z = \partial\tilde{\theta}/\partial z = 0$. At the surface, the instantaneous wall shear stress and scalar flux are computed using Monin–Obukhov similarity theory (Businger et al., 1971). Although this theory was developed for mean quantities, it is common practice in LES to use it for instantaneous (filtered) variables (e.g., Schumann, 1975; Schmidt and Schumann, 1989; Moeng, 1984). One option (Schumann, 1975; Piomelli and Balaras, 2002) is to compute the instantaneous surface shear stress $\tau_{i3,w}$ as a function of the resolved velocity \tilde{u}_i at the grid point immediately above the surface (in our case, at a height $z = \Delta_z/2$), as follows:

$$\tau_{i3,w} = -u_*^2 \left[\frac{\tilde{u}_i}{U(z)} \right] \quad (i = 1, 2), \quad (11)$$

where u_* is the friction velocity, which is computed from the mean horizontal wind velocity $U(z) = \langle (\tilde{u}_1^2 + \tilde{u}_2^2)^{1/2} \rangle$ at the first level of grid points ($z = \Delta_z/2$) using Monin–Obukhov similarity theory. This classical boundary condition parameterization is common practice in LES of high-Reynolds number boundary layers and it guarantees that the average stress relates to the average velocity at the first vertical grid point according to Monin–Obukhov similarity theory. However, it is important to note that recent studies have shown that this approach can substantially misrepresent the level of fluctuations in the modelled surface shear stress (Marusic et al., 2001). We use it nonetheless since no universally agreed improved surface stress model has been developed to date, and in order not to confuse effects with the SGS modelling, which is the focus of the present work. Future work will address the interaction between the boundary condition formulation and the subgrid-scale model. As in Andren et al. (1994), the surface scalar flux $q_{3,w}$ is set to a constant and spatially uniform value $\langle q_{3,w} \rangle$.

In the lower boundary condition used to compute $\tau_{i3,w}$ (Equation (11)), u_* is taken to be 0.45 m s^{-1} , and the surface roughness length for momentum (z_o) is taken to be 0.1 m . As for the scalar flux boundary condition, the value of the constant average surface flux $\langle q_{3,w} \rangle$ used in the scalar flux boundary condition has no effect on the non-dimensionalized results presented below. The domain is divided into $N_x \times N_y \times N_z = 120 \times 120 \times 120$ nodes, and additional simulations are carried out with resolutions of $N_x \times N_y \times N_z = 24 \times 24 \times 24$, $36 \times 36 \times 36$, $54 \times 54 \times 54$, and $80 \times 80 \times 80$, in order to study the scale dependence of the model coefficient and the simulation results.

2.3. RESULTS

In this section we present results corresponding to the scalar fields (first-order and second-order statistics) as well as the value of the dynamic coefficient in the eddy-diffusion model, obtained from our simulations with the dynamic model. Since θ is a passive scalar, these results have no effect on the velocity field and the dynamic Smagorinsky model coefficient, which are described in detail by Porté-Agel et al.

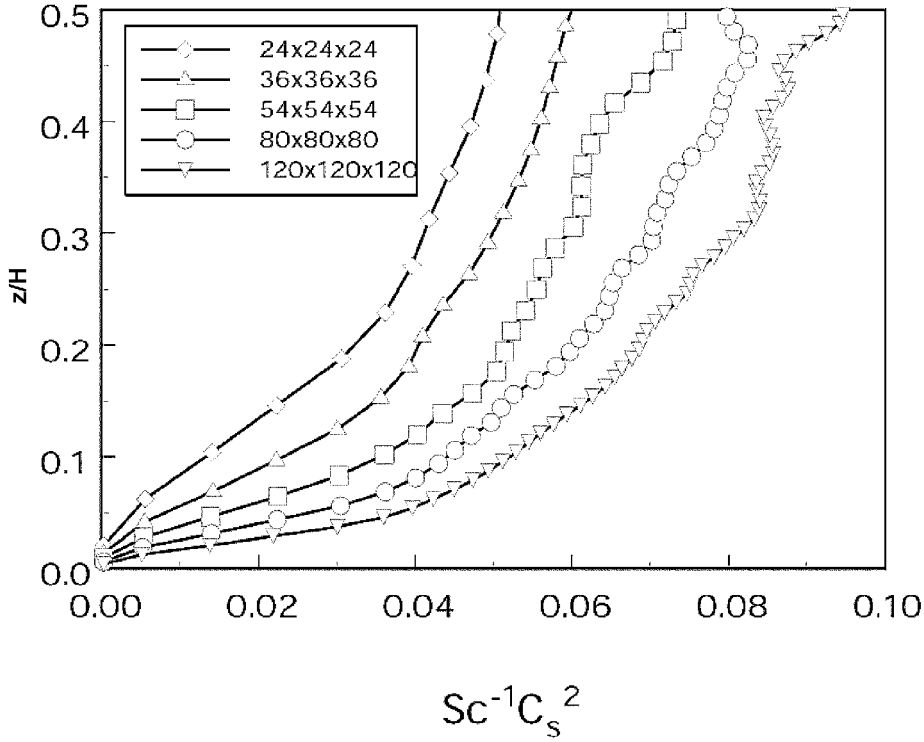


Figure 1. Dynamic coefficient $Sc_{sgs}^{-1}C_s^2$ as a function of z/H (ordinate), obtained from simulations with different resolutions.

(2000). Most of the results presented below correspond to averages over time and horizontal planes.

The value of the model coefficient $Sc_{sgs}^{-1}C_s^2$ returned by the dynamic model (Equation (8)) is presented in Figures 1 and 2. In order to examine the dependence of the dynamic coefficient on Δ we show results from four simulations that use the dynamic model with different resolutions ($24 \times 24 \times 24$, $36 \times 36 \times 36$, $54 \times 54 \times 54$, and $80 \times 80 \times 80$, and $120 \times 120 \times 120$ nodes, respectively). The value of the eddy-diffusion coefficient $Sc_{sgs}^{-1}C_s^2$ from the five simulations is presented in Figures 1 and 2 as a function of the distance to the surface z , normalized by the boundary-layer height H and the filter size Δ , respectively. The collapse of the five curves in Figure 2 indicates that the model coefficient is dependent on z/Δ . For any given Δ , we observe the expected reduction of the coefficient with decreasing z . However, at a fixed height z , $Sc_{sgs}^{-1}C_s^2$ depends on Δ , which is consistent with the results found by Porté-Agel et al. (2001) (also shown in Figure 2) using data from an a priori field study (with a fixed z and a variable Δ). Scale dependence appears to extend higher up in the boundary layer for $Sc_{sgs}^{-1}C_s^2$ than for C_s , which remains approximately scale invariant away from the ground for similar resolutions (Porté-Agel et al., 2000). This result indicates that away from the surface (large z/Δ) local

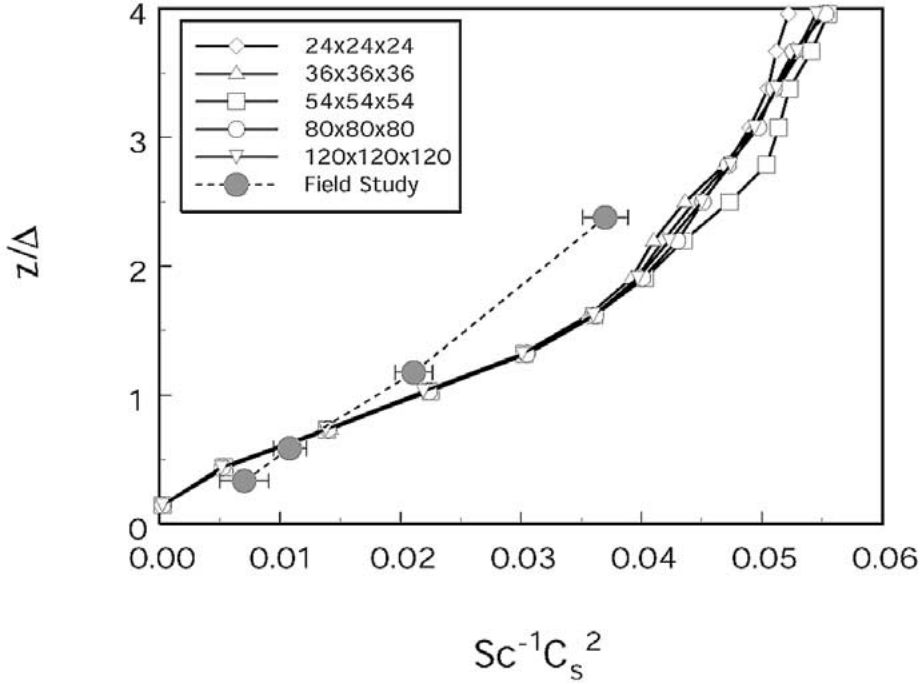


Figure 2. Dynamic coefficient $Sc_{gs}^{-1}C_s^2$ as a function of z/Δ , obtained from simulations with different resolutions (open symbols). Solid circles and corresponding error bars are results from an a priori field study (Porté-Agel et al., 2001).

isotropy, associated with scale-invariance of the coefficient, is well satisfied by the velocity but not by the scalar concentration for the grid aspect ratio and resolutions considered here. This is consistent with the idea that scalars are in general more anisotropic than the velocity field (Warhaft, 2000; Kang and Meneveau, 2001). It is also important to note that scale dependence of the model coefficient constitutes an internal inconsistency in the standard dynamic model since Figure 2 is obtained by assuming scale invariance. Therefore, it is of interest to generalize the dynamic models to include scale dependence.

Figures 3a and b show the non-dimensional vertical gradient of the mean scalar concentration

$$\Phi_\theta = \frac{kz}{\theta_*} \frac{d\langle\tilde{\theta}\rangle}{dz}$$

as a function of distance to the ground z , normalized by H and the grid scale Δ , respectively; k is the von Kármán constant ($k = 0.4$) and $\theta_* = -\langle q_{3,w} \rangle u_*^{-1}$. According to similarity theory (Businger et al., 1971) one expects that in the surface layer (approximately the lowest 10% of the boundary layer) Φ_θ has a constant value of 0.74. The combination of the eddy-viscosity and the eddy-diffusion mod-

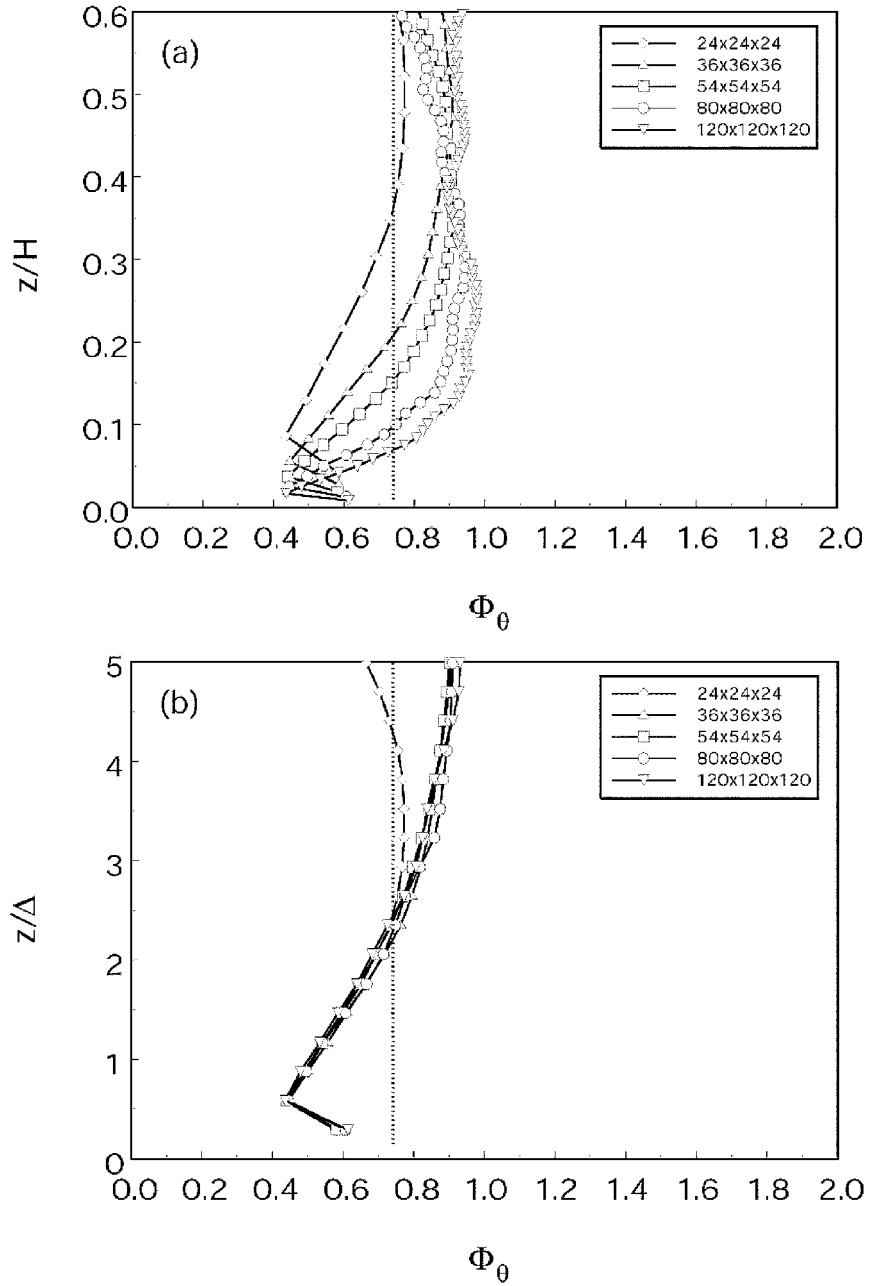


Figure 3. Non-dimensional vertical gradient of the mean scalar concentration ($\Phi_\theta = \frac{kz}{\theta_*} \frac{d(\bar{\theta})}{dz}$) as a function of height, from simulations with the traditional (scale-invariant) dynamic model using different resolutions. The height z is normalized with boundary layer depth H (a) and grid size Δ (b). The dotted line shows the value of 0.74 expected to hold throughout the surface layer ($z/H \lesssim 0.1$) according to similarity theory.

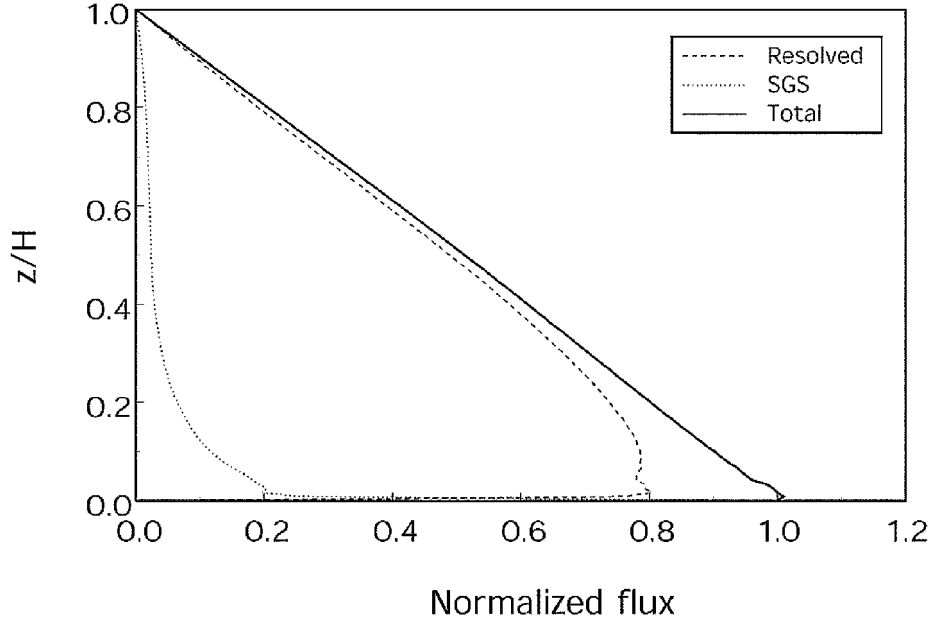


Figure 4. Vertical distribution of the resolved flux $\langle \tilde{u}'_3 \tilde{\theta}' \rangle$, SGS flux $\langle q_3 \rangle$ and total turbulent flux $\langle u'_3 \theta' \rangle = \langle \tilde{u}'_3 \tilde{\theta}' \rangle + \langle q_3 \rangle$, obtained from the simulations with the dynamic model. All the fluxes are normalized with $u_* \theta_*$.

els yields a value of Φ_θ that is too small near the ground, and increases too sharply in the surface layer (where Φ_θ is expected to remain constant). As in the case of the model coefficient (Figures 1 and 2), Φ_θ shows an unrealistic dependence on grid scale near the surface.

Figure 4 shows the vertical distribution of the resolved flux $\langle \tilde{u}'_3 \tilde{\theta}' \rangle$, SGS flux $\langle q_3 \rangle$ and total turbulent flux $\langle u'_3 \theta' \rangle = \langle \tilde{u}'_3 \tilde{\theta}' \rangle + \langle q_3 \rangle$, obtained from the $120 \times 120 \times 120$ -nodes simulations with the dynamic model. The fluxes and the height are normalized by $u_* \theta_*$ and H , respectively. Since a constant mean surface flux of value $\langle q_{3,w} \rangle = -u_* \theta_*$ is imposed, in the absence of viscous effects, the normalized averaged total turbulent (Reynolds) flux ($\langle u'_3 \theta' \rangle / (u_* \theta_*)$) decreases linearly from a value of 1 at the surface to a value of 0 at the top of the boundary layer.

The vertical distribution of the variance of the resolved scalar concentration $\langle \tilde{\theta}'^2 \rangle$ (where $\tilde{\theta}' = \tilde{\theta} - \langle \tilde{\theta} \rangle$) is presented in Figure 5. The level of resolved scalar variance is directly related to the level of SGS dissipation, i.e., the rate at which the resolved scalar variance is transferred from the resolved scales to the subgrid scales. The SGS dissipation rate is forced by the SGS model and it is defined as

$$\chi = -q_i \frac{\partial \tilde{\theta}}{\partial x_i}. \quad (12)$$

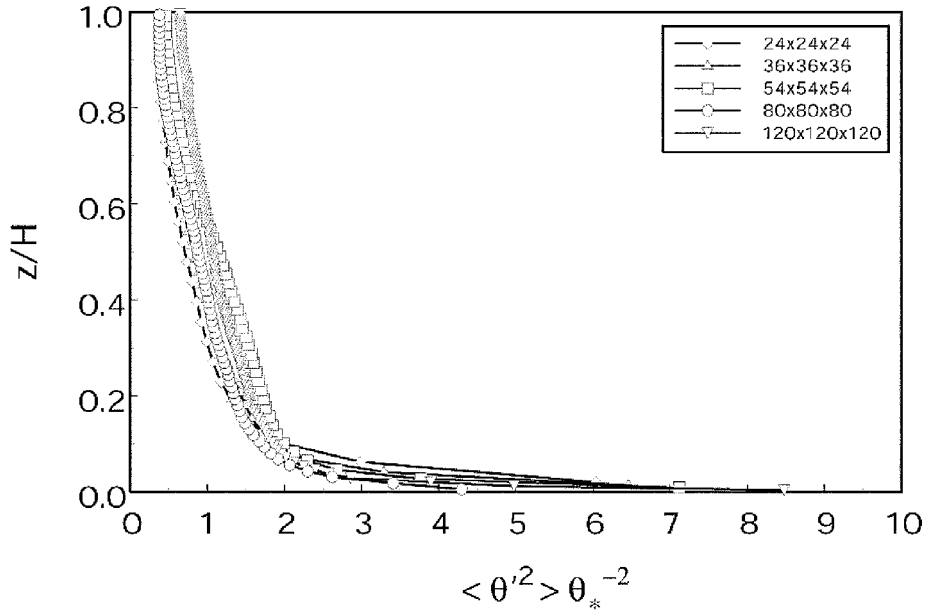


Figure 5. Vertical distribution of the non-dimensional variance of the resolved scalar concentration $\langle \tilde{\theta}^2 \rangle$, obtained from the simulations using the dynamic model with different resolutions. The variance is normalized with θ_*^2 .

For details on the derivation of Equation (12) in the context of the conservation equation for $\langle \tilde{\theta}^2 \rangle$ see Porté-Agel et al. (1998). Figure 6 shows the horizontally averaged value of the SGS dissipation of the scalar variance $\langle \chi \rangle = -\left\langle q_i \frac{\partial \tilde{\theta}}{\partial x_i} \right\rangle$ obtained at different heights. As expected, the average SGS dissipation is positive, indicating a net transfer of scalar variance from the resolved (larger) scales to the subgrid (smaller) scales. Also, $\langle \chi \rangle$ is larger near the ground due in part to the fact that the magnitude of both $\langle q_i \rangle$ and $\left\langle \frac{\partial \tilde{\theta}}{\partial x_i} \right\rangle$ is larger in that region.

In order to study the distribution of the resolved scalar variance at different scales, next we analyze the turbulent spectrum of the scalar concentration. Applying Kolmogorov arguments to the velocity and scalar concentration spectra, one expects that these spectra are proportional to $k_1^{-5/3}$ in the inertial subrange. In a neutrally stable ABL, there is experimental evidence that this inertial subrange extends for a range of relatively small scales, $k_1 \gtrsim z^{-1}$, where z is the measurement height and k_1 is the streamwise wavenumber (e.g., Kolmogorov, 1962; Saddoughi and Veeravalli, 1994). The averaged scalar spectra of $\tilde{\theta}$ computed at different heights ($\xi = z/H$) are shown in Figure 7. Spectra are calculated from one-dimensional Fourier transforms that are then averaged in the spanwise direction and also in time. Note that the spectra are normalized with θ_* and z , and plotted against $k_1 z$, in order to check for a possible collapse of the curves in the inertial subrange. For relatively small scales ($k_1 z \gtrsim 1$), at which Kolmogorov

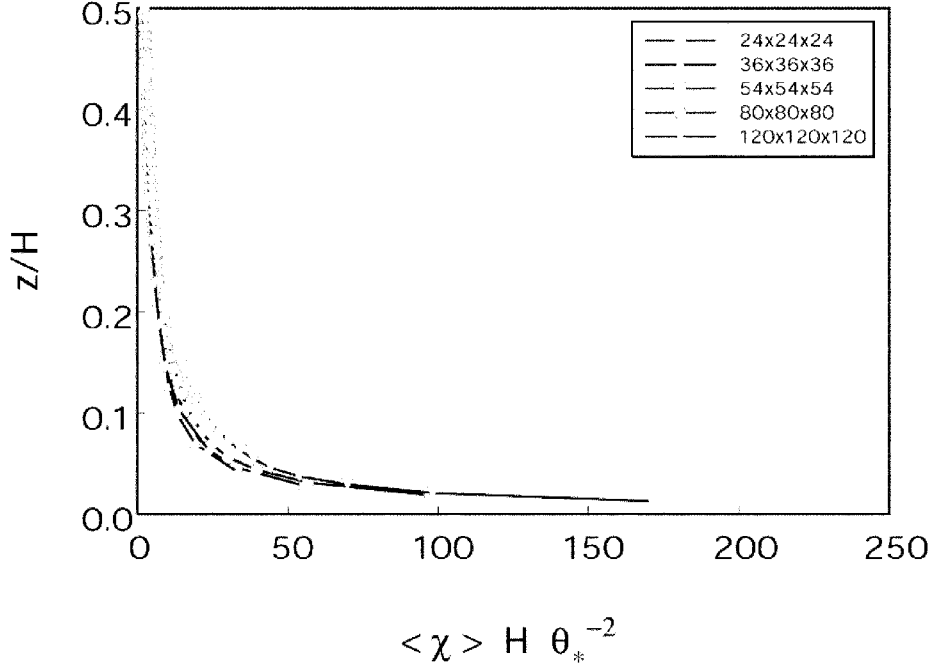


Figure 6. Vertical distribution of the non-dimensional SGS dissipation of the scalar variance $\langle \chi \rangle$, obtained from the simulations with the dynamic model. The SGS dissipation is normalized with $H\theta_*^{-2}$.

scaling arguments are expected to hold, the spectra show a relatively good collapse, with a slope close to the theoretical value of $-5/3$. Near the surface, where most of the resolved scales fall outside of the inertial subrange ($k_1 z \lesssim 1$) the slope of the computed spectra is very flat and shows an unrealistic pile-up of scalar variance at the smallest resolved scales.

3. The Scale-Dependent Dynamic Model

3.1. MODEL FORMULATION

Next, we present a generalization of the dynamic model to account for scale dependence of the model coefficient. Without assuming that $\mathcal{S}_{sgs}^{-1} C_S^2(\Delta) = \mathcal{S}_{sgs}^{-1} C_S^2(2\Delta)$ we can still apply the dynamic model given by Equations (3), (5) and (6). Note that this change introduces a new unknown $\beta_\theta \equiv \mathcal{S}_{sgs}^{-1} C_S^2(2\Delta) / \mathcal{S}_{sgs}^{-1} C_S^2(\Delta)$. For scale-invariant situations, $\beta_\theta = 1$. In order to compute $\mathcal{S}_{sgs}^{-1} C_S^2$ using Equation (8) we need to estimate β_θ . A dynamic value for β_θ can be obtained using a second test filter at scale $\hat{\Delta} > \bar{\Delta}$. For simplicity, and without loss of generality, we take $\hat{\Delta} = 4\Delta$, and denote variables filtered at scale

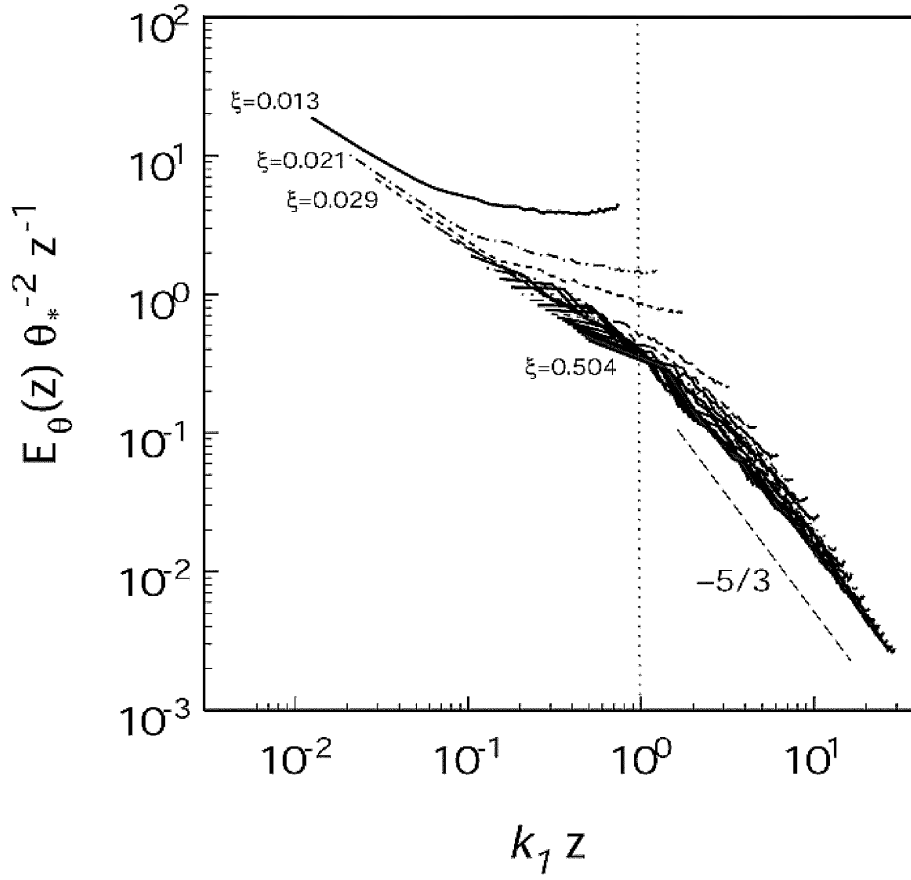


Figure 7. Normalized streamwise spectrum of the resolved scalar concentration $\tilde{\theta}$ versus $k_1 z$ at different heights. From top to bottom, the curves are for $\xi = z/H = 0.013, 0.021, 0.029, 0.054, 0.079, 0.104, 0.129, 0.154, 0.179, 0.204, 0.229, 0.254, 0.279, 0.304, 0.329, 0.354, 0.379, 0.404, 0.429, 0.454, 0.470, \text{ and } 0.504$. The dotted line shows the theoretical upper limit of the inertial subrange. The slope of $-5/3$ is also shown.

4Δ by a caret ($\hat{\quad}$). Similar to Equation (3), the resolved flux corresponding to scales between Δ and 4Δ can be written as

$$K'_i = Sc_{sgs}^{-1} C_S^2 X'_i, \quad (13)$$

where

$$K'_i = \widehat{\tilde{u}_i \tilde{\theta}} - \widehat{\tilde{u}_i} \widehat{\tilde{\theta}}, \quad (14)$$

and

$$X'_i = \Delta^2 \left(\widehat{\left| \tilde{S} \right| \frac{\partial \tilde{\theta}}{\partial x_i}} - 4^2 \frac{Sc_{sgs}^{-1} C_S^2 (4\Delta)}{Sc_{sgs}^{-1} C_S^2 (\Delta)} \widehat{\tilde{S}} \left| \frac{\partial \tilde{\theta}}{\partial x_i} \right| \right). \quad (15)$$

Again minimizing the error as in Section 2 yields, besides Equation (8), another equation for $S c_{sgs}^{-1} C_S^2(\Delta)$:

$$S c_{sgs}^{-1} C_S^2(\Delta) = \frac{\langle K'_i X'_i \rangle}{\langle X'_i X'_i \rangle}. \quad (16)$$

Setting Equation (8) equal to Equation (16) yields

$$\langle K_i X_i \rangle \langle X'_i X'_i \rangle - \langle K'_i X'_i \rangle \langle X_i X_i \rangle = 0, \quad (17)$$

which has two unknowns, $\beta_\theta = S c_{sgs}^{-1} C_S^2(2\Delta) / S c_{sgs}^{-1} C_S^2(\Delta)$ and $\gamma = S c_{sgs}^{-1} C_S^2(4\Delta) / S c_{sgs}^{-1} C_S^2(\Delta)$. In order to close the system, a relationship between β_θ and γ is required. Thus, a functional form of the scale dependence of the coefficient needs to be postulated. As in Porté-Agel et al (2000), we assume a power law of the form $S c_{sgs}^{-1} C_S^2(\Delta) \sim \Delta^\phi$, or, in a dimensionally appropriate way,

$$S c_{sgs}^{-1} C_S^2(\alpha\Delta) = S c_{sgs}^{-1} C_S^2(\Delta) \alpha^\phi. \quad (18)$$

For such a power-law behaviour, β_θ does not depend on scale and is equal to $\beta_\theta = 2^\phi$. Note that this assumption is much weaker than the standard dynamic model, which corresponds to the special case $\phi = 0$. We stress that one does not need to assume the power law to hold over a wide range of scales, but only between scales Δ and 4Δ . A consequence of the assumed local power law is that $S c_{sgs}^{-1} C_S^2(2\Delta) / S c_{sgs}^{-1} C_S^2(\Delta) = S c_{sgs}^{-1} C_S^2(4\Delta) / S c_{sgs}^{-1} C_S^2(2\Delta) = \beta_\theta$, and thus $\gamma = S c_{sgs}^{-1} C_S^2(4\Delta) / S c_{sgs}^{-1} C_S^2(\Delta) = \beta_\theta^2$. With this substitution Equation (17) only contains the unknown β_θ , and can be rewritten as a fifth-order polynomial on β_θ :

$$P(\beta_\theta) \equiv A_0 + A_1 \beta_\theta + A_2 \beta_\theta^2 + A_3 \beta_\theta^3 + A_4 \beta_\theta^4 + A_5 \beta_\theta^5 = 0. \quad (19)$$

The coefficients in Equation (19) can be obtained from:

$$\begin{aligned} A_0 &= b_2 c_1 - b_1 c_2, \quad A_1 = a_1 c_2 - b_2 e_1, \quad A_2 = b_2 d_1 + b_1 e_2 - a_2 c_1, \\ A_3 &= a_2 e_1 - a_1 e_2, \quad A_4 = -a_2 d_1 - b_1 d_2, \quad \text{and } A_5 = a_1 d_2, \end{aligned} \quad (20)$$

where

$$\begin{aligned} a_1 &= -\Delta^2 4 \left\langle \left| \tilde{S} \right| \frac{\partial \tilde{\theta}}{\partial x_i} K_i \right\rangle, \\ b_1 &= -\Delta^2 \left\langle \left| \tilde{S} \right| \frac{\partial \tilde{\theta}}{\partial x_i} K_i \right\rangle, \end{aligned}$$

$$\begin{aligned}
c_1 &= \Delta^4 \left\langle \overline{|\tilde{S}| \frac{\partial \tilde{\theta}}{\partial x_i}} \overline{|\tilde{S}| \frac{\partial \tilde{\theta}}{\partial x_i}} \right\rangle, \\
d_1 &= \Delta^4 (4)^2 \left\langle \overline{|\tilde{S}|^2 \frac{\partial \tilde{\theta}}{\partial x_i} \frac{\partial \tilde{\theta}}{\partial x_i}} \right\rangle, \text{ and} \\
e_1 &= 2\Delta^4 4 \left\langle \overline{|\tilde{S}| \frac{\partial \tilde{\theta}}{\partial x_i}} \overline{|\tilde{S}| \frac{\partial \tilde{\theta}}{\partial x_i}} \right\rangle
\end{aligned} \tag{21}$$

are also already needed for the traditional dynamic model, and

$$\begin{aligned}
a_2 &= -\Delta^2 4^2 \left\langle \widehat{\left| \tilde{S} \right| \frac{\partial \tilde{\theta}}{\partial x_i} K'_i} \right\rangle, \\
b_2 &= -\Delta^2 \left\langle \widehat{\left| \tilde{S} \right| \frac{\partial \tilde{\theta}}{\partial x_i} K'_i} \right\rangle, \\
c_2 &= \Delta^4 \left\langle \widehat{\left| \tilde{S} \right| \frac{\partial \tilde{\theta}}{\partial x_i}} \widehat{\left| \tilde{S} \right| \frac{\partial \tilde{\theta}}{\partial x_i}} \right\rangle, \\
d_2 &= \Delta^4 (4)^2 \left\langle \widehat{\left| \tilde{S} \right|^2 \frac{\partial \tilde{\theta}}{\partial x_i} \frac{\partial \tilde{\theta}}{\partial x_i}} \right\rangle, \text{ and} \\
e_2 &= 2\Delta^4 (4)^2 \left\langle \widehat{\left| \tilde{S} \right| \frac{\partial \tilde{\theta}}{\partial x_i}} \widehat{\left| \tilde{S} \right| \frac{\partial \tilde{\theta}}{\partial x_i}} \right\rangle
\end{aligned} \tag{22}$$

are new required terms for the scale-dependent model.

One can show that only the largest root is physically viable. A Newton–Raphson method is used to find that root. Once β_θ has been computed, it is used in Equation (6) to compute X_i , which in turn is used in Equation (8) to obtain $S_{sgs}^{-1} C_S^2(\Delta)$.

3.2. RESULTS

The scale-dependent dynamic model is applied to compute C_S in the Smagorinsky model (as in Porté-Agel et al., 2000) and $S_{sgs}^{-1} C_S^2$ in the eddy-diffusion model (as described above) in simulations of the same neutral atmospheric boundary layer with a constant scalar flux presented in Section 2. The scale-dependent coefficients are computed every 10 time steps. We found that the scale-dependent dynamic models take only about 5% more CPU time than the traditional dynamic models.

Figures 8a and 8b show the time averaged values of the scale-dependent parameters $\beta_\theta = Sc_{sgs}^{-1} C_S^2(2\Delta) / Sc_{sgs}^{-1} C_S^2(\Delta)$ and $\beta = C_S^2(2\Delta) / C_S^2(\Delta)$ as functions of the normalized heights z/H and z/Δ , respectively. In the interior of the flow β_θ is clearly dependent on resolution and smaller than one ($\beta \approx 0.8$ for the highest resolutions), indicating that for the resolutions under consideration $Sc_{sgs}^{-1} C_S^2$ remains scale dependent even far from the surface. This contrasts with the scale invariance observed for the Smagorinsky coefficient ($\beta \approx 1$ for all resolutions) in that region. This is consistent with the results presented in Figures 1 and 2, and it agrees with the fact that anisotropy in turbulent flows is stronger for scalars than for the velocity field (Warhaft, 2000; Kang and Meneveau, 2001).

The average values of the coefficients $Sc_{sgs}^{-1} C_S^2$, C_S and Sc_{sgs} , obtained from our simulations with the scale-dependent dynamic models, are shown in Figures 9a–c as a function of normalized height z/Δ . The values of $Sc_{sgs}^{-1} C_S^2$ and C_S are computed using the scale-dependent dynamic procedures, and the subgrid-scale Schmidt number Sc_{sgs} is calculated by dividing C_S^2 by $Sc_{sgs}^{-1} C_S^2$. These results are compared with the average value of the coefficients that result from the scale-invariant dynamic model using a resolution of $120 \times 120 \times 120$ nodes (also shown in Figure 2 for $Sc_{sgs}^{-1} C_S^2$). Also presented in Figure 9 are the values of the coefficients obtained from an a priori field study on subgrid-scale heat fluxes (Porté-Agel et al., 2001). Figures 9a–c show a clear dependence of all coefficients on the nondimensional ratio z/Δ , with a relatively good collapse of the results from the highest resolutions ($54 \times 54 \times 54$ and higher). For relatively small values of the z/Δ ratio ($0 \lesssim z/\Delta \lesssim 2$), an increase in z/Δ is associated with robust increases in $Sc_{sgs}^{-1} C_S^2$ (from $Sc_{sgs}^{-1} C_S^2 \approx 0$ to $Sc_{sgs}^{-1} C_S^2 \approx 0.05$) and C_S (from 0 to $C_S \approx 0.14$), and a decrease in Sc_{sgs} (from $Sc_{sgs} \approx 0.6$ for $z/\Delta \approx 0.15$ to $Sc_{sgs} \approx 0.3$ for $z/\Delta \approx 2$). These trends are in good qualitative agreement with results from the a-priori field study (solid circles in Figure 9). For $z/\Delta \gtrsim 2$, C_S becomes nearly scale invariant and has a value of $C_S \approx 0.14$. In contrast, $Sc_{sgs}^{-1} C_S^2$, and consequently Sc_{sgs} , remain scale dependent for relatively large values of z/Δ . It is important to note that the SGS Schmidt number obtained with the scale-invariant model (dashed line in Figure 9c) shows an unrealistic dependence on z/Δ near the ground. In particular, the scale-invariant dynamic coefficient decreases from $Sc_{sgs} \approx 0.5$ at the lowest point to $Sc_{sgs} \approx 0.2$ at $z/\Delta \approx 0.7$, and then it increases with increasing z/Δ to reach a value of $Sc_{sgs} \approx 0.3$ at $z/\Delta \approx 0.15$.

The averaged non-dimensional scalar concentration gradient

$$\Phi_\theta = \frac{kz d\langle\tilde{\theta}\rangle}{\theta_* dz},$$

from the scale-dependent dynamic model (symbols) and the standard dynamic model (dashed line) are shown in Figure 10. The scale-dependent dynamic model yields values of Φ_θ that are more realistic than the ones obtained with the scale-invariant dynamic model (Figure 3). In particular, Φ_θ remains scale invariant and closer to a constant value in the surface layer, which is more consistent with the

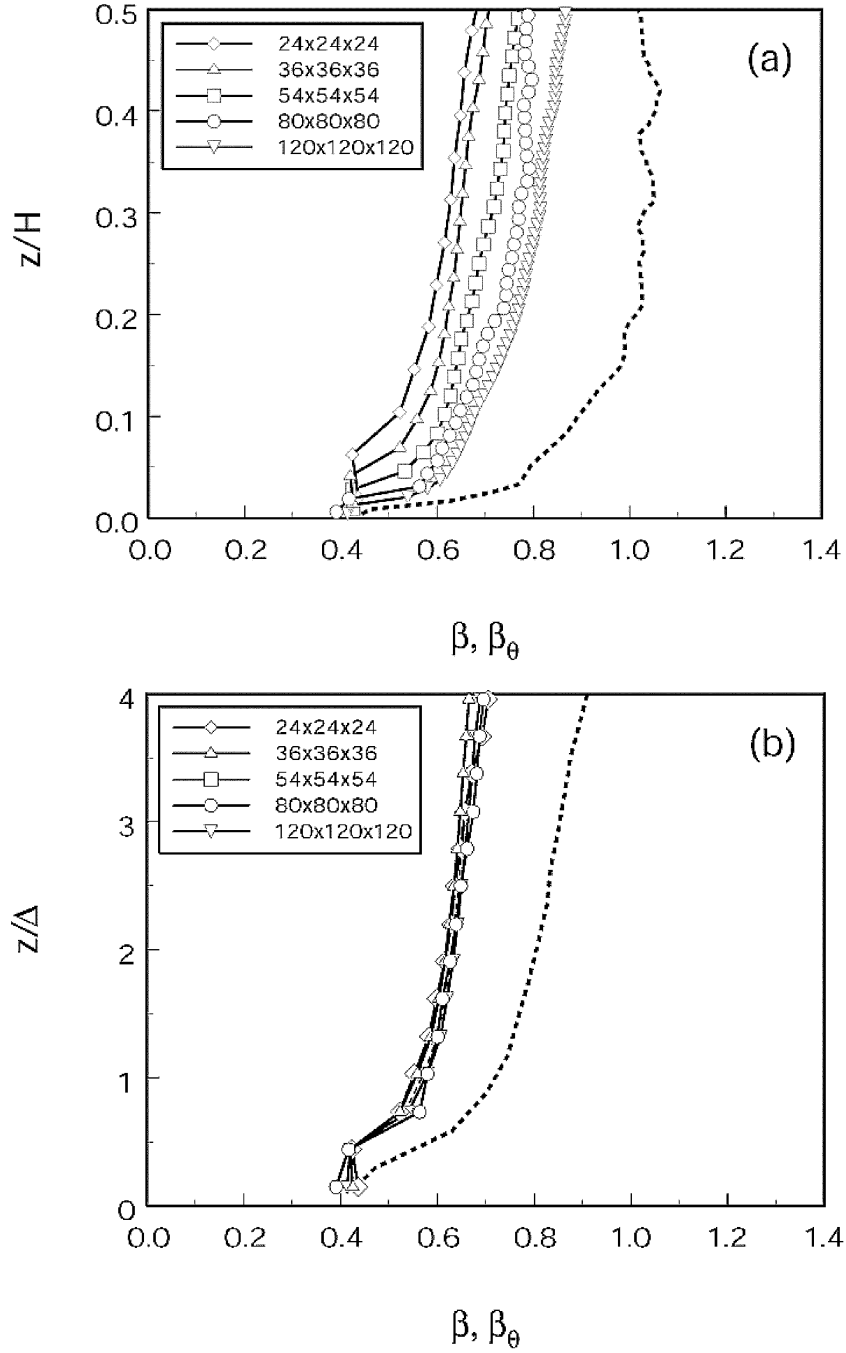


Figure 8. Time averaged values of the scale-dependent parameter $\beta_\theta = Sc_{sgs}^{-1} C_S^2(2\Delta) / Sc_{sgs}^{-1} C_S^2(\Delta)$ as a function of the normalized height z/H (a) and z/Δ (b) for different resolutions (open symbols). The dashed line shows the value of $\beta = C_S^2(2\Delta) / C_S^2(\Delta)$ from the $120 \times 120 \times 120$ -nodes simulation.

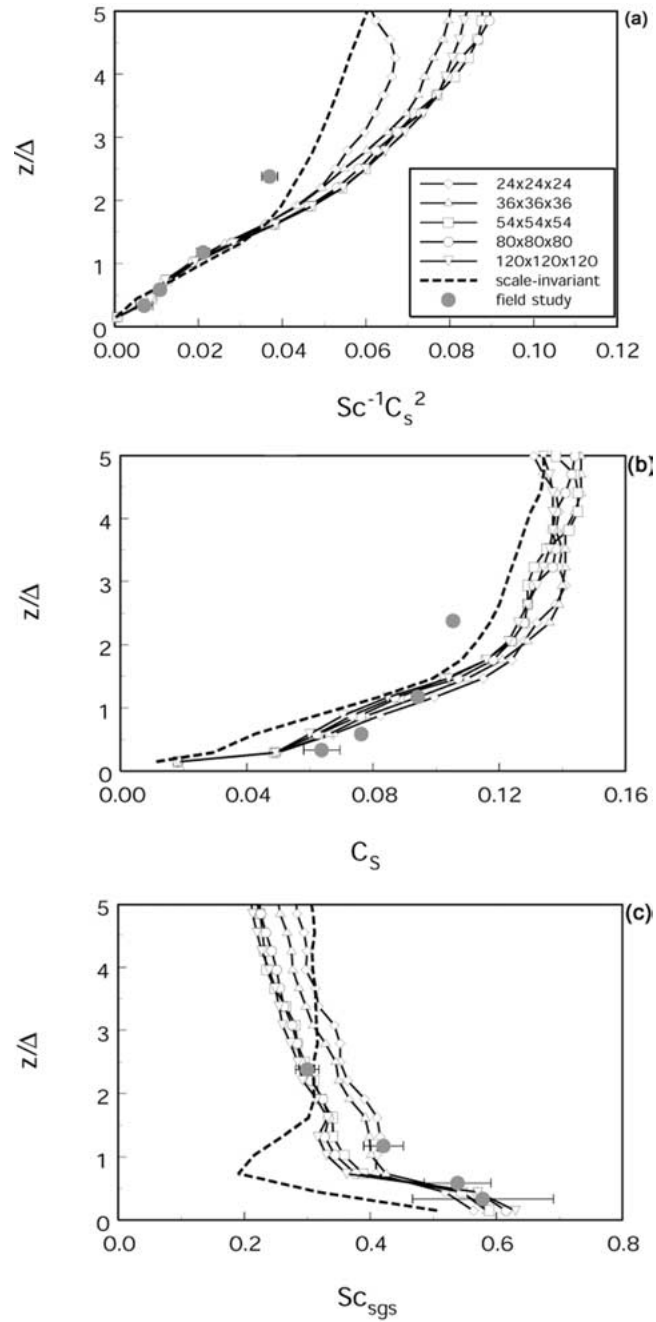


Figure 9. Vertical distribution of the time-averaged value of the coefficients $Sc_{sgs}^{-1}C_s^2$ (a), C_s (b), and Sc_{sgs} (c), obtained using the scale dependent dynamic model using different resolutions (open symbols). Results from the scale-invariant dynamic model with a resolution of $120 \times 120 \times 120$ nodes are also included (dashed line). Solid circles and corresponding error bars are results from an a priori field study (Porté-Agel et al., 2001).

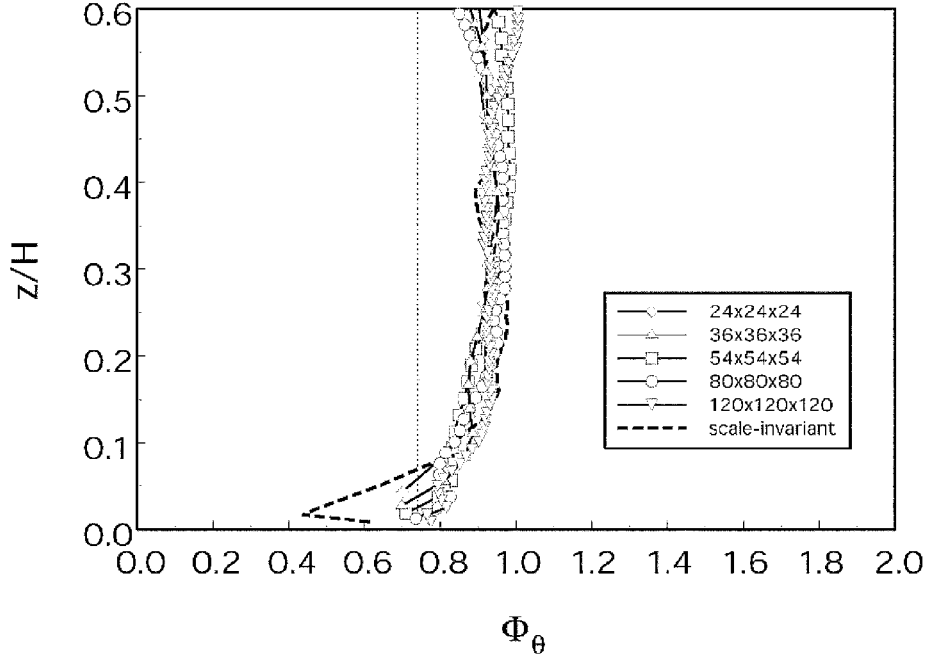


Figure 10. Non-dimensional vertical gradient of the mean scalar concentration ($\Phi_\theta = \frac{kz}{\theta_*} \frac{d\langle\tilde{\theta}\rangle}{dz}$) from simulations with the scale-dependent dynamic model. The dotted line shows the value of 0.74 expected to hold throughout the surface layer ($z/H \lesssim 0.1$) according to similarity theory. Results from the scale-invariant dynamic model with a resolution of $120 \times 120 \times 120$ nodes are also included (dashed line).

expected logarithmic profile. The value of Φ_θ in that layer is slightly larger than the expected value of 0.74. A similar departure (from the expected value of 1.0) is found for the non-dimensional velocity gradient,

$$\Phi = \frac{kz}{u_*} \frac{d\langle U \rangle}{dz}$$

– see Porté-Agel et al. (2000) for details – consistent with a value of the von Karman constant slightly smaller than 0.4 ($k \approx 0.36$). Also, as expected, Φ_θ increases progressively as we move away from the surface into the so-called wake region.

Figure 11 shows the vertical distribution of the resolved flux $\langle \tilde{u}_3 \tilde{\theta}' \rangle$, SGS flux $\langle q_3 \rangle$ and total turbulent flux $\langle u_3' \theta' \rangle = \langle \tilde{u}_1 \tilde{\theta}' \rangle + \langle q_3 \rangle$, obtained from the simulations using the scale-dependent dynamic model. It is important to note that near the ground, the relative contribution of the SGS fluxes to the total turbulent fluxes is larger for the scale-dependent dynamic model than for the scale-invariant dynamic model. This can be understood considering the fact that both the model coefficients and the vertical gradients are larger in magnitude in simulations with the scale-dependent dynamic model.

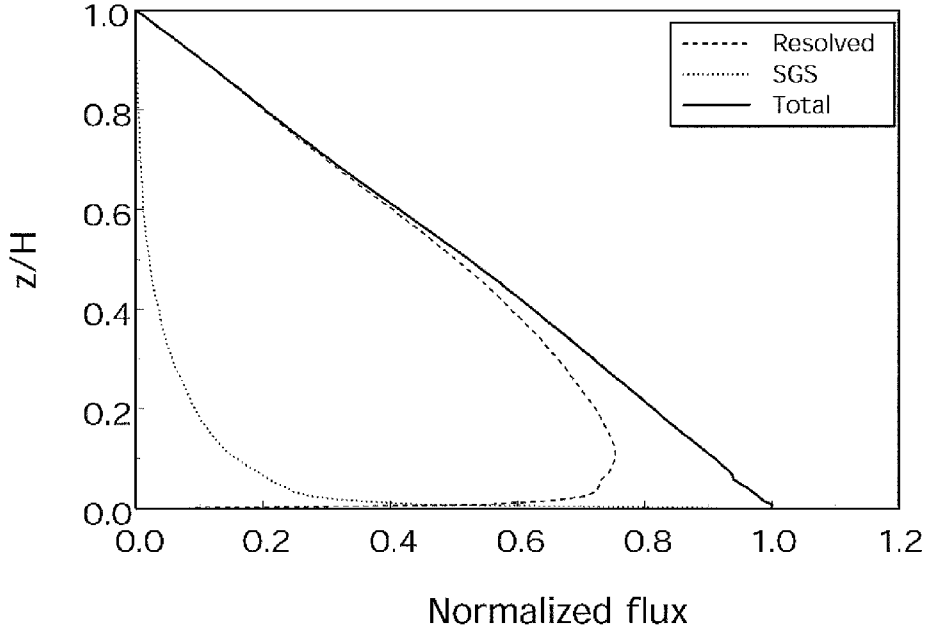


Figure 11. Vertical distribution of the resolved flux $\langle \tilde{u}'_3 \tilde{\theta}' \rangle$, SGS flux $\langle q_3 \rangle$ and total turbulent flux $\langle u'_3 \theta' \rangle = \langle \tilde{u}'_3 \tilde{\theta}' \rangle + \langle q_3 \rangle$, obtained from the simulations with the scale-dependent dynamic model. All the fluxes are normalized with $u_* \theta_*$.

The vertical distribution of the variance of the scalar concentration $\langle \tilde{\theta}^2 \rangle$ and the SGS dissipation of the scalar variance $\langle \chi \rangle$ obtained with the scale-dependent dynamic model are presented in Figures 12 and 13, respectively, and compared with the results from the scale-invariant dynamic model (dashed line). Near the ground, the scale-dependent dynamic model is more dissipative (larger $\langle \chi \rangle$), and it is associated with larger values of the resolved scalar variance.

The averaged scalar spectra obtained from the $120 \times 120 \times 120$ -nodes simulation using the scale-dependent model at different vertical positions ($\xi = z/H$) in the ABL are shown in Figure 14. As before, the spectra are averaged in the spanwise direction and in time, and they are normalized with θ_* and z . Figure 14 shows a clear $k_1^{-5/3}$ scaling for relatively small scales ($k_1 z \gtrsim 1$), with a good collapse (slightly better than in Figure 7 for the scale-invariant dynamic model) of all curves at those scales. As in Figure 7, near the surface, where the grid and/or test-filter scale fall near the limit or outside of the inertial subrange (most of the resolved scales satisfy $k_1 z \lesssim 1$), spectra show an unrealistically high temperature variance at the smallest resolved scales. However, this excess appears to be weaker, affecting a smaller range of scales compared with spectra from the scale-invariant dynamic model (Figure 7). These results suggest that near the surface the scale-dependent model is better able to reproduce the rate of transfer of scalar variance towards the subgrid scales than the dynamic model, which is not dissipative enough. We

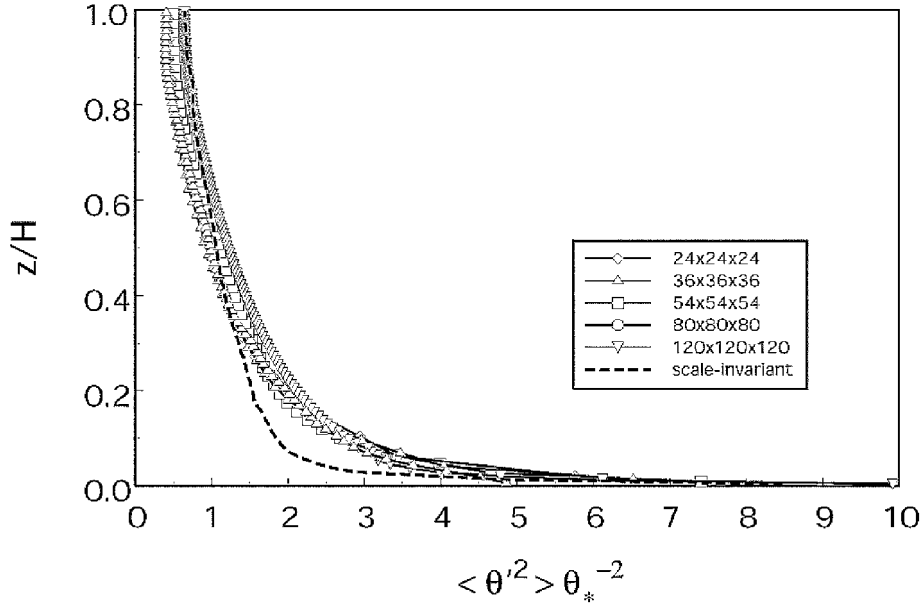


Figure 12. Vertical distribution of the non-dimensional variance of the resolved scalar concentration $\langle \tilde{\theta}'^2 \rangle$, obtained from the simulations with the scale-dependent dynamic model. Results from the scale-invariant dynamic model with a resolution of $120 \times 120 \times 120$ nodes are also included (dashed line). The variance is normalized with θ_*^2 .

conclude that this, together with the improved mean flow statistics (more consistent with surface-layer similarity theory) and the more realistic dependence of the dynamic coefficients on z/Δ , makes the scale-dependent dynamic model a desirable choice in simulations of high-Reynolds number boundary layers.

4. Summary

A modification of the dynamic model is presented that accounts for scale dependence of the lumped coefficient ($Sc_{sgs}^{-1} C_S^2$) in the eddy-diffusion SGS model. Motivation for including scale dependence is presented from simulations of a neutral ABL with a constant flux of a passive scalar, using the traditional (scale-invariant) dynamic model. The dependence of the model coefficient obtained from our simulations is consistent with previous results from an a priori field study (Porté-Agel et al., 2001). Scale dependence is stronger near the ground where the filter and/or test filter scales are comparable to the distance to the ground, falling near (or even outside) the upper limit of the inertial subrange. Scale dependence is also found to be stronger for $Sc_{sgs}^{-1} C_S^2$ than for the coefficient in the eddy-viscosity model (C_S^2) due to the stronger anisotropic behaviour of the scalars compared to the velocity field.

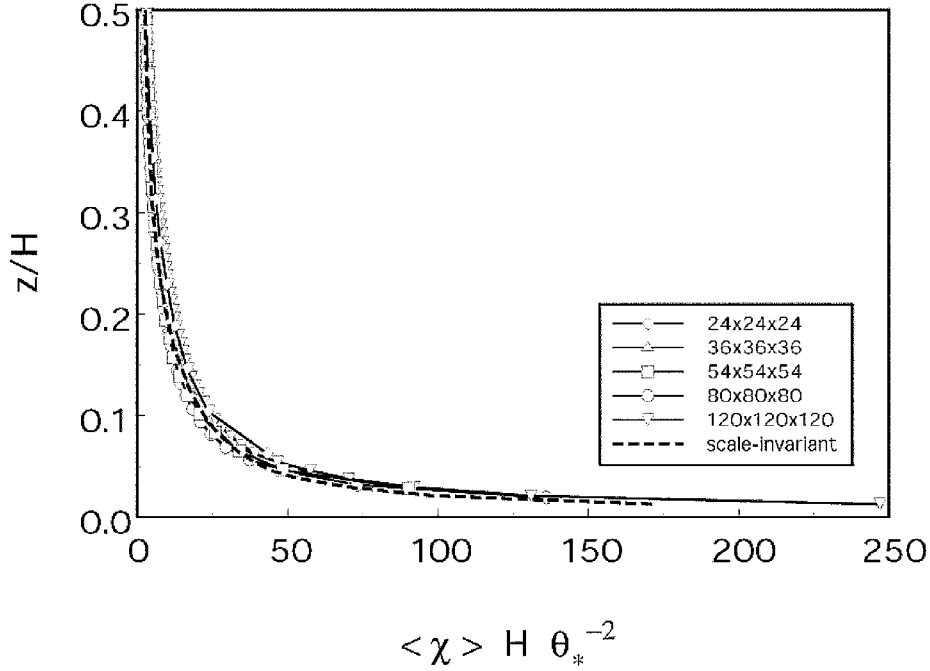


Figure 13. Vertical distribution of the non-dimensional SGS dissipation of the scalar variance $\langle \chi \rangle$, obtained from the simulations with the scale-dependent dynamic model. Results from the scale-invariant dynamic model with a resolution of $120 \times 120 \times 120$ nodes are also included (dashed line). The SGS dissipation is normalized with $H\theta_*^{-2}$.

The new scale-dependent model is fully dynamic, i.e., it does not require any parameter specification or tuning, since the model coefficient is computed from the dynamics of the resolved scales. Moreover, it allows for scale dependence of the coefficient in a self-consistent way. Simulations with the new model are stable and robust, and yield expected trends of the coefficient as a function of scale. Results from our simulations of a neutral ABL with a constant surface flux of a passive scalar show improved mean concentration profiles and scalar spectra compared with the traditional (scale-invariant) dynamic model.

Future work will extend the implementation of the scale-dependent dynamic procedure to active scalars (temperature), other base models (e.g., mixed model, Lagrangian model), and to other flow conditions where scale dependence of the model coefficient is expected. In particular, the new scale-dependent procedures are expected to better capture the dynamics of the flow in boundary layers with strong stable stratification (e.g., the nocturnal boundary layer and inversion layers) and/or high degree of surface heterogeneity (e.g., changing topography and land cover).

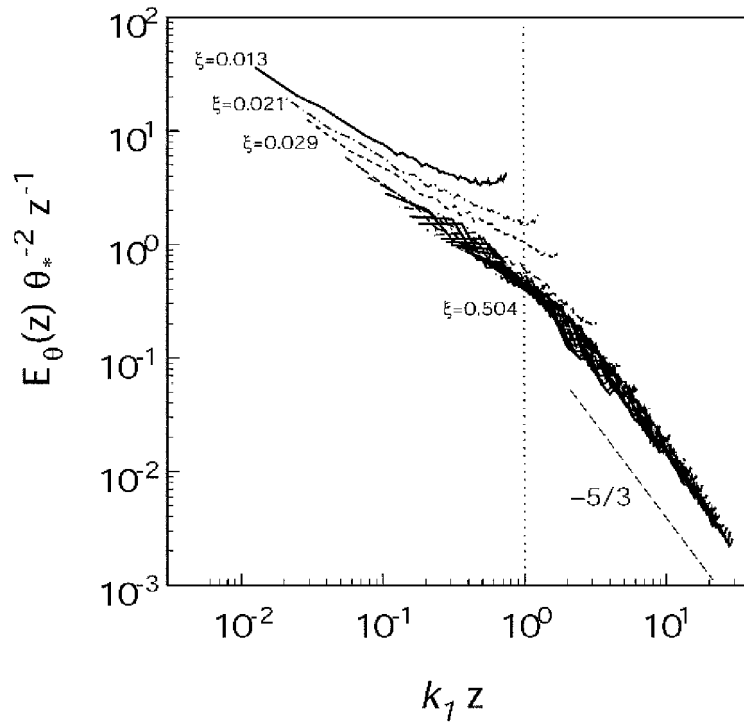


Figure 14. Normalized streamwise spectrum of the resolved scalar concentration $\tilde{\theta}$ versus $k_1 z$ at different normalized heights, using the proposed scale-dependent dynamic model. From top to bottom, the curves are for $\xi = z/H = 0.013, 0.021, 0.029, 0.054, 0.079, 0.104, 0.129, 0.154, 0.179, 0.204, 0.229, 0.254, 0.279, 0.304, 0.329, 0.354, 0.379, 0.404, 0.429, 0.454, 0.470,$ and 0.504 . The dotted line shows the theoretical upper limit of the inertial subrange. The slope of $-5/3$ is also shown.

Acknowledgements

This work was supported by NSF (grant EAR-0094200) and NASA (grants NAG5-10569 and NAG5-11801). Computer resources were provided by the Minnesota Supercomputing Institute.

References

- Albertson, J. D. and Parlange, M. B.: 1999, 'Natural Integration of Scalar Fluxes from Complex Terrain', *Adv. Water Res.* **23**, 239–252.
- Andren, A., Brown, A. R., Graf, J., Mason, P. J., Moeng, C.-H., Nieuwstadt, F. T. M., and Schumann, U.: 1994, 'Large-Eddy Simulation of the Neutrally Stratified Boundary Layer: A Comparison of Four Computer Codes', *Quart. J. Roy. Meteorol. Soc.* **120**, 1457–1484.
- Avissar, R. and Schmidt, T.: 1998, 'An Evaluation of the Scale at which Ground-Surface Heat Flux Patchiness Affects the Convective Boundary Layer Using Large-Eddy Simulations', *J. Atmos. Sci.* **55**, 2666–2689.

- Businger, J. A., Wyngaard, J. C., Izumi, Y., and Bradley, E. F.: 1971, 'Flux-Profile Relationships in the Atmospheric Surface Layer', *J. Atmos. Sci.* **28**, 181–158.
- Canuto, C., Hussaini, M. Y., Quarteroni, A., and Zang, T. A.: 1988, *Spectral Methods in Fluid Dynamics* (Springer Series on Computational Physics), Springer Verlag, 557 pp.
- Canuto, V. M. and Cheng, Y.: 1997, 'Determination of the Smagorinsky–Lilly Constant C_S ', *Phys. Fluids* **9**, 1368–1378.
- Deardorff, J. W.: 1971, 'On the Magnitude of the Subgrid-Scale Eddy Coefficient', *J. Comp. Phys.* **7**, 120–133.
- Deardorff, J. W.: 1980, 'Stratocumulus-Capped Mixed Layers Derived from a Three-Dimensional Model', *Boundary-Layer Meteorol.* **18**, 495–527.
- Germano, M., Piomelli, U., Moin, P., and Cabot, W. H.: 1991, 'A Dynamic Subgrid-Scale Eddy Viscosity Model', *Phys. Fluids* **3**, 1760–1765.
- Ghosal, S., Lund, T., Moin, P., and Akselvoll, K.: 1995, 'A Dynamic Localization Model for Large-Eddy Simulation of Turbulent Flows', *J. Fluid Mech.* **286**, 229–255.
- Hunt, J. C. R., Stretch, D. D., and Britter, R. E.: 1988, 'Length Scales in Stably Stratified Turbulent Flows and their Use in Turbulence Models', in J. S. Puttock (ed.), *Stably Stratified Flows and Gas Dynamics*, Clarendon Press, Oxford.
- Kang, H. S. and Meneveau, C.: 2001, 'Passive Scalar Anisotropy in a Heated Turbulent Wake: New Observations and Implications for LES', *J. Fluid Mech.* **442**, 161–170.
- Kleissl, J., Meneveau, C., and Parlange, M. B.: 2003, 'On the Magnitude and Variability of Subgrid-Scale Eddy-Diffusion Coefficients in the Atmospheric Surface Layer', *J. Atmos. Sci.* **60**, 2372–2388.
- Kolmogorov, A. N.: 1962, 'A Refinement of Previous Hypotheses Concerning the Local Structure of Turbulence in a Viscous Incompressible Fluid at High Reynolds Number', *J. Fluid Mech.* **13**, 82–85.
- Kosovic, B.: 1997, 'Subgrid-Scale Modelling for the Large-Eddy Simulation of High-Reynolds-Number Boundary Layers', *J. Fluid Mech.* **336**, 151–182.
- Lilly, D. K.: 1967, 'The Representation of Small-Scale Turbulence in Numerical Simulation Experiments', in *Proceedings of the IBM Scientific Computing Symposium on Environmental Sciences*, IBM form no. 320-1951, White Plains, New York, pp. 195–209.
- Lilly, D. K.: 1992, 'A Proposed Modification of the Germano Subgrid-Scale Closure Method', *Phys. Fluids A* **4**, 633–635.
- Lin, C. L. and Glendening, J. W.: 2002, 'Large Eddy Simulation of an Inhomogeneous Atmospheric Boundary Layer under Neutral Conditions', *J. Atmos. Sci.* **59**, 2479–2497.
- Marusic, I., Kunkel, G. J., and Porté-Agel, F.: 2001, 'Experimental Study of Wall Boundary Conditions for Large Eddy Simulation', *J. Fluid Mech.* **446**, 309–320.
- Mason, P. J. and Derbyshire, S. H.: 1990, 'Large-Eddy Simulation of the Stably-Stratified Atmospheric Boundary Layer', *Boundary-Layer Meteorol.* **53**, 117–162.
- Meneveau, C. and Katz, J.: 2000, 'Scale-Invariance and Turbulence Models for Large-Eddy Simulation', *Annu. Rev. Fluid Mech.* **32**, 1–32.
- Meneveau, C. and Lund, T. S.: 1997, 'The Dynamic Smagorinsky Model and Scale-Dependent Coefficients in the Viscous Range of Turbulence', *Phys. Fluids* **9**, 3932–3934.
- Meneveau, C., Lund, T. S., and Cabot, W.: 1996, 'A Lagrangian Dynamic Subgrid-Scale Model of Turbulence', *J. Fluid Mech.* **319**, 353–385.
- Moeng, C.-H.: 1984, 'A Large-Eddy Simulation Model for the Study of Planetary Boundary-Layer Turbulence', *J. Atmos. Sci.* **46**, 2311–2330.
- Moin, P., Squires, K. D., and Lee, S.: 1991, 'A Dynamic Subgrid-Scale Model for Compressible Turbulence and Scalar Transport', *Phys. Fluids* **3**, 2746–2757.
- Nieuwstadt, F. T. M., Mason, P. J., Moeng, C.-H., and Schumann, U.: 1991, 'Large-Eddy Simulation of the Convective Boundary Layer: A Comparison of Four Computer Codes', *Turbulent Shear Flows*, **8**, 343–367.

- Orszag, S. A. and Pao, Y.-H.: 1974, 'Numerical Computation of Turbulent Shear Flows', *Adv. Geophys.* **18A**, 224–236.
- Piomelli, U.: 1999, 'Large-Eddy Simulation: Achievements and Challenges', *Prog. Aerosp. Sci.* **35**, 335–362.
- Piomelli, U. and Balaras, E.: 2002, 'Wall-Layer Models for Large-Eddy Simulations', *Annu. Rev. Fluid Mech.* **34**, 349–374.
- Porté-Agel, F., Meneveau, C., and Parlange, M. B.: 1998, 'Some Basic Properties of the Surrogate Subgrid-Scale Heat Flux in the Atmospheric Boundary Layer', *Boundary-Layer Meteorol.* **88**, 425–444.
- Porté-Agel, F., Meneveau, C., and Parlange, M. B.: 2000, 'A Scale-Dependent Dynamic Model for Large-Eddy Simulation: Application to a Neutral Atmospheric Boundary Layer', *J. Fluid Mech.* **415**, 261–284.
- Porté-Agel, F., Pahlow, M., Meneveau, C., and Parlange, M. B.: 2001, 'Atmospheric Stability Effect on Subgrid-Scale Physics for Large-Eddy Simulation', *Adv. Water Res.* **24**, 1085–1102.
- Saddoughi, G. and Veeravalli, S. V.: 1994, 'Local Isotropy in Turbulent Boundary Layers at High Reynolds Number', *J. Fluid Mech.* **268**, 333–372.
- Schmidt, H. and Schumann, U.: 1989, 'Coherent Structure of the Convective Boundary Layer Derived from Large-Eddy Simulations', *J. Fluid Mech.* **200**, 511–562.
- Schumann, U.: 1975, 'Subgrid Scale Model for Finite Difference Simulations of Turbulent Flows in Plane Channels and Annuli', *J. Comp. Phys.* **18**, 376–404.
- Schumann, U.: 1991, 'Subgrid Length-scales for Large-eddy Simulation of Stratified Turbulence', *Theor. Comp. Fluid Dyn.* **2**, 279–290.
- Shaw, R. H. and Schumann, U.: 1992, 'Large-Eddy Simulation of Turbulent Flow above and within a Forest', *Boundary-Layer Meteorol.* **61**, 47–64.
- Sullivan, P. P., McWilliams, J. C., and Moeng, C.-H.: 1994, 'A Subgrid-Scale Model for Large-Eddy Simulation of Planetary Boundary-Layer Flows', *Boundary-Layer Meteorol.* **71**, 247–276.
- Warhaft, Z.: 2000, 'Passive Scalars in Turbulent Flows', *Annu. Rev. Fluid Mech.* **32**, 203–240.

